Atmospheric Environment 339 (2024) 120872

Contents lists available at ScienceDirect

Atmospheric Environment

journal homepage: www.elsevier.com/locate/atmosenv

Intercomparison of WRF-chem aerosol schemes during a dry Saharan dust outbreak in Southern Iberian Peninsula

Miguel Pino-Carmona [a,*], José A. Ruiz-Arias [b], Sol Fernández-Carvelo [a,c], Juan A. Bravo-Aranda [a,c], Lucas Alados-Arboledas [a,c]

[a] Department of Applied Physics, University of Granada, Granada, Spain
[b] Departamento de Física Aplicada I, Universidad de Málaga, Málaga, Spain
[c] Andalusian Institute for Earth System Research (IISTA-CEAMA), Granada, Spain

HIGHLIGHTS

- WRF-chem aerosol schemes yield distinct results simulating a dry dust outbreak in southern Spain on July 2021.
- Results with GOCART are more consistent with observations of dust optical properties and size distribution.
- MOSAIC and MADE present issues related with the representation of mineral dust size distribution.

ARTICLE INFO

Keywords:
WRF-Chem
Dust outbreak
Aerosol scheme
Comparison
Ångström's wavelength exponent
Lidar

ABSTRACT

The Iberian Peninsula (IP), where this study is conducted, has experienced an increase of the frequency and intensity of Saharan aerosol dust outbreaks over the latest decades, which may have an impact on its regional climate. The Weather Research and Forecasting model coupled with chemistry (WRF-chem) has been used worldwide to simulate dust outbreaks and can support the analysis of such potential impacts. However, it includes multiple alternative aerosol parameterization choices that have not been conveniently evaluated in the study region yet. Here, three of the most popular WRF-chem aerosol parameterization schemes, namely, the Goddard Chemistry Aerosol Radiation and Transport (GOCART), the Model for Simulating Aerosol Interactions and Chemistry (MOSAIC) and the Modal Aerosol Dynamics Model for Europe (MADE) schemes, are intercompared during a strong and dry dust outbreak on July 2021 in southern IP. The results show that the three schemes predict qualitatively similar dust intrusion patterns that are consistent with ground observations and have inter-model dust loading differences smaller than 4%. However, their average dust size distributions differ notably. While GOCART is reasonably consistent with observations, MOSAIC underpredicts the amount of dust particles with sub-micron diameters and overpredicts that of large particles and MADE does the opposite. This is found to have a strong detrimental impact on the prediction performance of dust optical properties in MOSAIC and MADE, which is related, at least partially, with issues in the required inter-sectional redistribution of dust parameters during the dust emission and calculation of optical properties. Overall, GOCART generally appears a better choice for strong and dry dust outbreak events in southern IP. It remains to be evaluated during wet dust outbreaks, which is a work underway.

1. Introduction

Aerosols are fundamental atmospheric constituents that take a principal role in a multitude of processes. Their importance for the atmosphere's fate, even at the global scale, is nowadays well recognized by the latest IPCC reports (Intergovernmental Panel On Climate Change, 2023), where aerosols have been found a major source of uncertainty, and thus of concern, in climate weather simulations. The typology of aerosols is wide and diverse as they enter directly into the atmosphere from multiple sources (e.g., dust, sea salt, volcanic eruptions, biogenic emissions, anthropogenic emissions) and form from interactions between themselves and/or other atmospheric constituents. By way of

* Corresponding author. Granada, 18006, Spain.
E-mail address: miguelpino@ugr.es (M. Pino-Carmona).

https://doi.org/10.1016/j.atmosenv.2024.120872
Received 6 May 2024; Received in revised form 16 August 2024; Accepted 12 October 2024
Available online 15 October 2024

consequence, they are found in a wide spectrum of concentrations, sizes, shapes and optical properties, which explains their utmost importance for processes in the micro- and macro-scales.

Most of the impacts of aerosols are regarded as direct or indirect. The former refers to the aerosol-radiation interactions, fundamentally, the ability of aerosols to absorb and scatter light photons (Bellouin et al., 2005). The latter, the so-called indirect effect, refers to the intricate aerosol-cloud interactions by which aerosols influence the formation, dissipation and optical properties of clouds (Albrecht, 1989; Lohmann and Feichter, 2005; Twomey, 1977). In addition to those two, there is a third kind of aerosol impact, known as semidirect, that refers to the change of moisture and cloud patterns in the atmosphere by a change of temperature originated from direct aerosol impacts (Amiri-Farahani et al., 2019).

Among atmospheric aerosols, mineral dust, whose main sources are deserts, is the most abundant species. Globally, the Sahara Desert is the most important one, with an estimated mineral dust emission flux into the atmosphere of 400–2200 Tg/yr (Huneeus et al., 2011). Mineral dust originates principally in alluvial processes, which results in a wide variety of dust particle sizes and compositions. The opacity of dust contributes notably to the atmospheric radiative forcing (Saidou Chaibou et al., 2020b) but its overall effects on cloud formation and precipitation are still subject of debate. It is highly hydrophobic, which favors the formation of ice nuclei (Weger et al., 2018; Zhang et al., 2011) and contributes to precipitation suppression (Rosenfeld et al., 2001). Nevertheless, as dust particles can be large enough to enhance the formation of CCN, the multiple processes that alter the dust physical and chemical properties during its transport within the atmosphere can ultimately affect the precipitation triggering processes (Bègue et al., 2015; Karydis et al., 2011, p. 1; Su and Fung, 2018; Tsarpalis et al., 2020).

Besides its very important role in atmospheric processes, mineral dust also has a substantial impact on air quality and human health (Díaz et al., 2017; Esmaeil et al., 2014), renewable energies (Kazem et al., 2014; Maghami et al., 2016), air transportation (Ryder et al., 2023), new particle formation events and the cloud condensation nuclei budget (Casquero-Vera et al., 2023), and in biological processes (Nogueira et al., 2021), to name a few. Hence, understanding the mineral dust emission, transport, interaction and deposition processes in the atmosphere is of utmost importance (Knippertz and Stuut, 2014). This is especially true in the Iberian Peninsula (IP), where this study is conducted, and where an increase of the frequency and intensity of aerosol dust outbreaks has recently been identified over the latest 70 years mainly influenced by the supplies of the adjoining Saharan Desert (Salvador et al., 2022).

Modern numerical weather models allow simulating all or some of the atmospheric processes related to mineral dust, thus being extremely useful to improve our understanding of those processes. Among the weather models that are capable of simulating the atmospheric chemistry, the Weather Research and Forecast model (WRF) coupled with chemistry (WRF-chem) is one of the most widely used (Grell et al., 2005). WRF-chem is a state-of-the-art community mesoscale non-hydrostatic weather model that simulates the emission, formation, transport, interaction and deposition of particles and gases and their feedback with the meteorological fields (Fast et al., 2006). The model counts with multiple physical configuration options that must be set up for each specific application. In particular, WRF-chem implements different physical formulations to simulate the aerosol interactions in the atmosphere, referred to as aerosol parameterization (AP) schemes, among which the most popular are: the Goddard Chemistry Aerosol Radiation and Transport (GOCART) scheme (Chin et al., 2000; Ginoux et al., 2001), the Model for Simulating Aerosol Interactions and Chemistry (MOSAIC) scheme (Zaveri et al., 2008), and the Modal Aerosol Dynamics Model for Europe (MADE) scheme (Ackermann et al., 1998). They have remarkable differences including, e.g., the type and number of aerosol species considered, the treatment of the aerosol size distributions, and the interactions with other atmospheric components. Among them, the differences in the treatment of the aerosol size distribution are of significant relevance. While MADE uses a modal representation of aerosols, MOSAIC is sectional and GOCART is bulk, except for sea salt and mineral dust that are sectional. A more detailed description of these schemes is provided in Section 2.3.

The entrainment of mineral dust into the atmosphere is parameterized with the dust emission (DE) scheme, whose role is critical to simulate the dust loading and size distribution in the atmosphere (LeGrand et al., 2019; Parajuli et al., 2019; Ukhov et al., 2021). The DE scheme is coupled to the AP scheme and, in particular, must use the same representation as that AP scheme for the dust size distribution (i.e., bulk, sectional or modal).

The WRF-chem's GOCART AP scheme, which has been recently reviewed and improved (Ukhov et al., 2021), is probably the most popular. It has been extensively used to simulate various aspects of mineral dust such as potential sources (Mesbahzadeh et al., 2020), outbreaks (Morichetti et al., 2020), long-term evolution (Jenkins and Gueye, 2022) or radiative forcing (Saidou Chaibou et al., 2020a; Zhao et al., 2010), as well as other aspects related to the model's configuration (Gueye and Jenkins, 2019; Palacios-Peña et al., 2019). The DE schemes that are available in WRF-chem have also been extensively evaluated and inter-compared in the literature, most often coupled to the GOCART aerosol scheme (Eltahan et al., 2018; Saidou Chaibou et al., 2020a; Yuan et al., 2019; Zhao et al., 2010). However, the number of studies that have addressed the sensitivity of dust simulations to the choice of WRF-chem's AP scheme is comparatively much smaller and, to these authors' knowledge, none of them considers GOCART, MOSAIC and MADE at the same time, and none is focused in the Western Mediterranean basin or the IP (Bran et al., 2022; Bucaram and Bowman, 2021; Georgiou et al., 2018; Palacios-Peña et al., 2019; Palacios-Peña et al., 2020; Rizza et al., 2017; Rizza et al., 2018; Rizza et al., 2023; Zhao et al., 2010).

This work evaluates the performance of the GOCART, MOSAIC and MADE WRF-chem's AP schemes to simulate a strong *dry* aerosol dust outbreak (ADO) (i.e., with no—or negligible—interaction with clouds) during the summer 2021 in southern IP. The study focuses on a dry event to minimize the potential aerosol indirect interactions and ultimately revolve around the drag and transport of mineral dust over the study region. The potential indirect impact of mineral dust in the region will be evaluated in a subsequent study. Since the choice of different DE schemes for the different AP schemes might affect the comparative results, all the aerosol schemes are coupled with the GOCART DE scheme, which is the only one that can be coupled with the three aerosol schemes. Furthermore, to reduce its potential detrimental performance impact, a preliminary calibration analysis is conducted as detailed in Section 3.1.

The WRF-chem's predictions are evaluated against ground observations of aerosol microphysical and optical properties gathered at The Andalusian Global ObseRvatory of the Atmosphere (AGORA) a Singular Laboratory of Advanced Technologies of the University of Granada (Spain) located in Southern Spain (Section 2.2). To that aim, a major research hypothesis is that the aerosol mineral dust dominates over other aerosol species during the ADO event, and thus, all observations are mostly representative of mineral dust. At this stage, the model validation is based only on ground observations (i.e., observations from sensors aboard satellites are not considered here) as they provide a more reliable and comprehensive description of dust aerosols, which is deemed more suitable for the purposes of this work, even if they are local and not regional.

The work is organized as follows. Section 2 describes the study region and the dry ADO event, presents the validation data and briefly summarizes the WRF-chem AP schemes and the GOCART DE scheme, as well as the model's configuration for the experiments. Section 3 presents the study results and Section 4 the main conclusions.

2. Data and methods

2.1. Study region and July 2021 ADO

The study is conducted in southeastern IP, which is exposed to tens of Saharan dust intrusion episodes every year, especially during summer (Mandija et al., 2017; Salvador et al., 2022). In particular, the number of events during July for the period 2006–2016 exceeded 200 (Russo et al., 2020).

According to the NOAA's Global Climate Report,[1] July 2021 was hot and dry in northern Africa and southern IP. There were two strong ADO episodes, the second one being the studied here. In the IP, the episode lasted three days, from 2021 to 07–22 to 2021-07-24 (Fig. 1), during which there were two peaks: one, sharper, about the start of the event on the midnight of 2021–07-22, and another, wider, during the last day. The atmospheric transport of dust evolved westward from the Sahara Desert, but part of it turned northward to approach the IP as it came over the Canary Islands (Fig. 1).

Alternatively, Fig. 2 depicts the July 2021 ADO event as simulated by WRF-chem using observations from the NASA's MODIS instrument, which offer a clearer picture of the intensity of the event.

2.2. Validation data

The observational dataset was collected in the Andalusian Global Atmosphere Observatory (AGORA) facilities[2] in the city of Granada and in the nearby Sierra Nevada mountains. AGORA is part of ACTRIS_ERIC (Aerosols, Clouds, and Trace gases Research InfraStructure Network, https://www.actris.eu/) (Laj et al., 2024) research infrastructure. The city, located within the Western Mediterranean basin (Fig. 2) and prone to orographic aerosol stagnation (Patrón et al., 2017), is affected by frequent long-range transport of Saharan dust (Fernández et al., 2019; Soupiona et al., 2019) as well as occasional biomass burning from nearby and distant sources (Alados-Arboledas et al., 2011; Ortiz-Amezcua et al., 2017). The AGORA facilities include active and passive remote sensing state-of-the-art instrumentation spread over three ground stations located at different altitudes. Data from two of these sites, University of Granada (UGR) and Cerro Poyos, are used in this study (Granados-Muñoz et al., 2020). The former is placed at the Andalusian Institute for Earth System Research/IISTA-CEAMA in the city (37.17° N, 3.60° W; 680 m a.s.l.). The latter is in the mountains (37.11° N, 3.49° W; 1820 m a.s.l.), approximately 25 km horizontally away from the UGR site.

The observational dataset includes aerosol optical depth (AOD) and inversion data from the Aerosol Robotic Network (AERONET; Giles et al., 2019) stations of Granada and Cerro Poyos. The datasets are publicly available at https://aeronet.gsfc.nasa.gov. AERONET is a global radiometric network that has been providing ground measurements of optical and microphysical properties of aerosols for more than 25 years and, overall, constitutes the highest-quality source of such data worldwide. The data used here are from the Version 3 "All points" dataset with quality level 2.0 for the optical data and level 1.5 for the inversion data since no significant differences were observed in this latter case between the two quality levels (see Sinyuk et al., 2020, for further details, including measurement uncertainties). In particular, the AOD observations at 440, 675, 870 and 1020 nm and the Ångström's wavelength exponent (AE) in the spectral range 440–870 nm were all retrieved from the direct sun measurements, while the volume size distribution (dV/dln(r), in $\mu m^3/\mu m^2$) was retrieved from the inversion product (almucantar sky scan scenario) for 22 radii spanning the range 0.005−15 μm. From this size distribution, the total dust amount, or total dust load, L_d (in $\mu m^3/\mu m^2$), is evaluated as:

$$L_d = \int_{0.005\ \mu m}^{15\ \mu m} \frac{dV}{d\ln r} d\ln r \quad (1)$$

In addition, the observational dataset includes measurements of the vertical structure of the atmosphere from two collocated instruments with the AERONET station in Granada. The first instrument is a ceilometer[3] from the E-PROFILE (https://e-profile.eu) program of the European Meteorological Network (EUMETNET; http://www.eumetnet.eu) that observes attenuated backscattering at 1064 nm (further details available in Cazorla et al., 2017). The second is the lidar Raman multiespectral (MULHACEN) from the European Aerosol Research Lidar Network (Pappalardo et al., 2014) (EARLINET; https://www.earlinet.org) and now part of the ACTRIS-ERIC infrastructure, that provides observations of backscattering at 355, 532 and 1064 nm (Guerrero-Rascado et al., 2008, 2009).

The AERONET data from the Cerro Poyos station are used in Section 3.1 for the GOCART DE scheme calibration. All other analyses use data gathered only at Granada, which is in a flat area at a lower height than the Cerro Poyos site in the mountains. Thus, the observations in Granada sweep a deeper atmospheric layer and prevent model errors related to the site altitude misrepresentation. In particular, the model altitude at Cerro Poyos is 1589 m a.s.l. But the actual altitude is 1809 m a.s.l. Conversely, the model and actual altitudes at Granada are 673 and 680 m a.s.l., respectively.

2.3. WRF-chem AP schemes

GOCART is a bulk model for all aerosol species (i.e., it does not resolve the particle size distribution) except for sea salt and dust, for which it has four and five sections, respectively. Instead, MOSAIC is sectional for all aerosol species and resolves the particle size distribution using eight sections (although a version with only four sections is also available, here, only the eight-sectional version is considered). Conversely, MADE performs a continuous parameterization of the aerosol size distribution using a three-modal distribution function (for the Aitken, accumulation and coarse modes) whose modal particle diameters evolve throughout time. Table 1 summarizes the main size parameters and density for mineral dust in each section (or mode, in the case of MADE) for the three AP schemes.

As the dust outbreak event considered here is dry, the microphysics parameterization is expected to take a negligible role in the removal of dust particles. However, this investigation is part of a bigger study in which wet events will be considered too, where processes such as wet deposition, wet scavenging, cloud condensation and ice nucleation, among others, need to be modeled. Hence, the WRF-chem physical setup used here tries to match as much as possible that one required for the wet events to be considered next. In addition, the choice of microphysics scheme in WRF-chem may be constrained by the choice of aerosol parameterization scheme too. All in all, both MOSAIC and MADE are here coupled with the Morrison 2-moment 6-class cloud microphysics scheme (Morrison et al., 2005) to simulate aqueous reactions, cloud chemistry and wet scavenging, while GOCART, which cannot be coupled with the Morrison scheme, is coupled with the Goddard 4-ice cloud microphysics scheme (Tao et al., 2019). This microphysics scheme is tailored for the GOCART AP scheme and allows the simulation of wet scavenging (*wetscav_onoff* = −1). Table 2 summarizes the aerosol and microphysics parameterization choices used in the WRF-chem simulations conducted here.

The three AP schemes share the aerosol optical scheme (*aer_op_opt=1*), which is based on the volume approximation method (Fast

[1] https://www.ncei.noaa.gov/access/monitoring/monthly-report/global/202107.

[2] https://atmosphere.ugr.es/en/about/presentation/agora.

[3] https://oscar.wmo.int/surface/index.html#/search/station/stationReportDetails/0-20008-0-UGR.

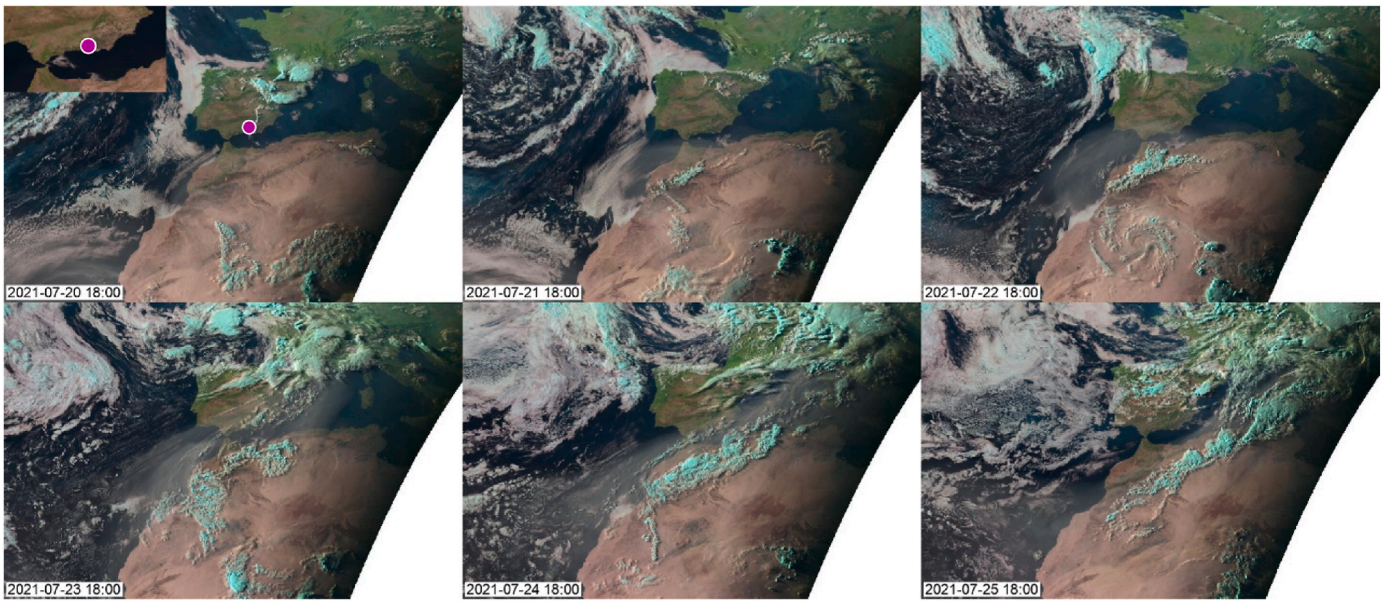

Fig. 1. July 2021 ADO event as viewed by the Natural Colour RGB EUMETSAT's product from Meteosat Second Generation satellite imagery. The panels sweep from 2021 to 07–20 18:00 UTC through 2021-07-25 18:00 UTC, in 24-h steps. The images are gathered from the EUMETView web portal (https://view.eumetsat.int/). Cyan clouds indicate a high content of ice crystals, while light-brown flows indicate dust. An in-depth explanation of colors system is provided in (https://user.eumetsat.int/resources/user-guides/natural-colour-rgb-quick-guide). The first panel indicates the location of the city of Granada with a purple point, zoomed in its left corner.

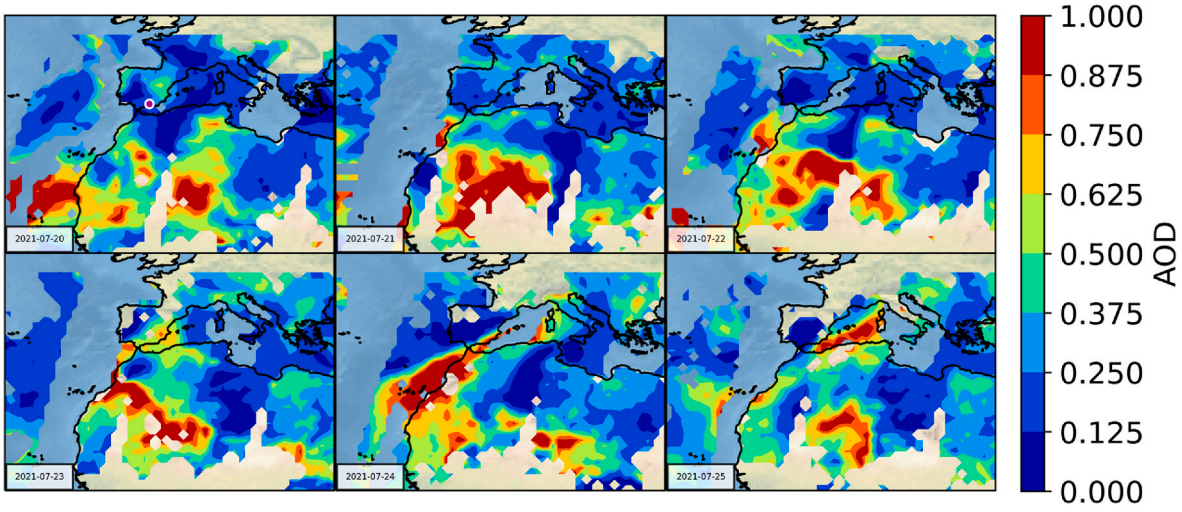

Fig. 2. ADO event as viewed by the Combined Dark Target and Deep Blue daily mean AOD at 0.55 μm for land and ocean products from the NASA's MODIS Level-3 Atmosphere Global Products. The panels sweep daily from 2021 to 07–20 through 2021-07-25 showing the daily mean AOD at 0.55 μm. The data were gathered from the NASA-GIOVANNI web portal (https://giovanni.gsfc.nasa.gov/giovanni/). The purple point indicates the location of the city of Granada.

et al., 2006). Originally, it was developed for MOSAIC, so the concentrations of aerosol species must be distributed into the eight MOSAIC sections. The volume-averaged diameter and the refractive index of all the species combined are calculated for each section. These averaged parameters are then introduced into a fast Mie scattering approximation model which evaluates the main aerosol optical properties at several wavelengths. It has been adapted to work also for GOCART and MADE using proper conversion weights from the 5 sections of GOCART and the 3 modes of MADE to the 8 MOSAIC sections.

2.4. The GOCART DE scheme

The WRF-chem's GOCART DE scheme was originally devised for the WRF-chem's GOCART AP scheme (Ginoux et al., 2001), thus both share the same five-sectional size distribution. The vertical dust mass emission flux for section k, F_k (kg m^{-2} s^{-1}), is evaluated as:

$$F_k = cSs_k u^2 (u - u_t) \quad (2)$$

where u is the horizontal wind speed at 10 m above the ground surface and u_t is the minimum wind speed to initiate the ground erosion, which is evaluated from the dust particles' diameter and soil characteristics and wetness (Ginoux et al., 2001; Marticorena and Bergametti, 1995). S is the dust's source function, which accounts for the dust availability on the ground at every grid cell, while s_k is the dust mass fraction of emitted sand, clay or silt in section k. Note that if $u < u_t$, F_k is negative meaning that there is no dust emission. A thorough review of this and two other dust emission schemes available in WRF-chem is provided in LeGrand et al. (2019). Last, but very important, c is a proportionality constant

Table 1
Mineral dust size parameters and density for the GOCART and MOSAIC sections and MADE modes in WRF-chem.

AP scheme	# of sections[a]	Section bounds[b] diameters (μm)	Mineral dust particle density (kg/m^3)
GOCART	5	0.2–2.0; 2.0–3.6; 3.6–6.0; 6–12; 12–20	2500, 2650, 2650, 2650, 2650
MOSAIC	8	0.039–0.078; 0.078–0.156; 0.156–0.312; 0.312–0.625; 0.625–1.25; 1.25–2.5; 2.5–5.0; 5–10	2500, 2500, 2500, 2650, 2650, 2650, 2650, 2650
MADE	3	0.01, 1.70 (Aitken); 0.07, 2.00 (Accumulation); 1.00, 2.50 (Coarse)	2500, 2600, 2600

[a] Modes in the case of MADE.
[b] Initial modal mean and standard deviation in the case of MADE.

Table 2
Aerosol parameterization schemes with their paired cloud microphysics schemes. See the WRF (https://www2.mmm.ucar.edu/wrf/users/docs/user_guide_v4/v4.2/) and WRF-chem (https://ruc.noaa.gov/wrf/wrf-chem/Users_guide.pdf) user guides for parameterization scheme details.

Configuration	Aerosol scheme and additional options	Cloud microphysics scheme
GOCART	GOCART simple (*chem_opt=300*)	Goddard 4-ice (*mp_physics=7*)
MOSAIC	8 bins MOSAIC with CBMZ chemical mechanism and aqueous reactions (*chem_opt=10*)	Morrison 2-moments (*mp_physics=10*)
MADE	MADE/SORGAM with RADM2 chemical mechanism and aqueous reactions (*chem_opt=11*)	Morrison 2-moments (*mp_physics=10*)

that is used to calibrate the emission flux (Gillette and Passi, 1988; LeGrand et al. (2019); Saidou Chaibou et al., 2020a). Apparently, as noted in the WRF-chem's code, its recommended value for the Sahara Desert is 0.65. However, its optimal value may depend on the immission study region.

As highlighted above, the GOCART DE scheme can be used in combination with the three AP schemes. When it is coupled with MOSAIC or MADE, the dust mass load, initially available only throughout the five GOCART DE scheme sections, is redistributed over the eight MOSAIC sections or the three MADE modes, respectively. In both cases, the total dust emitted within all GOCART sections is redistributed using a set of weights representing the percentage of dust assigned to each of the sections in MOSAIC, or modes in MADE.

2.5. WRF-chem experiments

All WRF-chem simulations are performed using the model version 4.2.1 with initial and boundary conditions provided by the European Centre for Medium-Range Weather Forecasts (ECMWF) ERA5 reanalysis (Hersbach et al., 2020). They cover the period from 2021 to 07–20 00:00 to 2021-07-26 00:00 with 1-h output time step, and 36 h of spin up. The spatial configuration consists of three nested domains with grid-cell sizes of 27, 9 and 3 km, respectively (Fig. 3).

All simulations use the same baseline physical configuration: revised MM5 Monin-Obukhov scheme for land surface processes and surface layer physics (*sf_sfclay_physics=1*), the Yonsei University scheme for the planetary boundary layer parameterization (*bl_pbl_physics=1*), the New Grell scheme for the cumulus parameterization (*cu_physics=5*), the Rapid Radiative Transfer Model (RRTMG) for both short-wave (*ra_sw_physics=4*) and long-wave (*ra_lw_physics=4*) radiation parameterizations, GOCART DE scheme (*dust_opt=1*), aerosol direct impact (*aer_rad_feedback=1*), aerosol aqueous effects (*wet_scav=0; cld_chem=0*), and aerosol optical properties using the volume approximation method

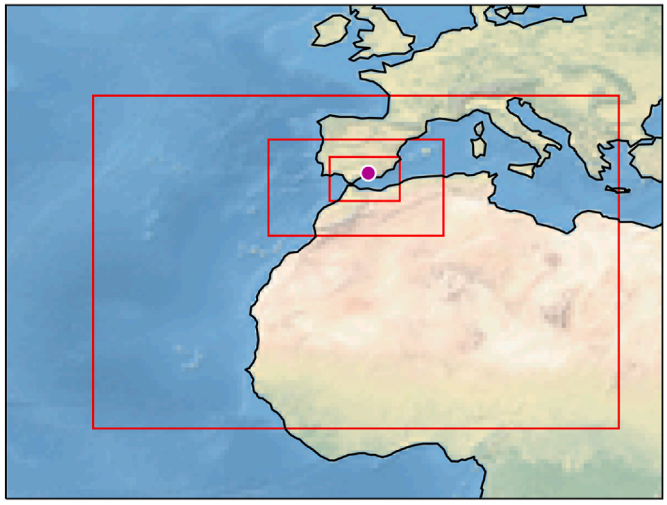

Fig. 3. Nested simulation domains. The purple point indicates the location of the city of Granada.

(*aer_op_opt=1*). Note that, unlike the microphysics scheme, the RRTMG scheme can be coupled with all AP schemes.

Combined with all previous setups, the WRF-chem model is alternatively run with the three aerosol and cloud microphysics configurations depicted in Table 2. The model results from the 3-km nested domain are then intercompared to each other and against the AERONET total-column and aerosol vertical profile observations described in Section 2.2. The three model runs use optimized values of the dust emission *c* parameter (Eq. (1)) which are determined from a previous round of four simulations using the GOCART aerosol configuration (see Table 2) with alternatively prescribed values for the *c* parameter: 0.40, 0.50, 0.65 and 0.80 (Section 3.1). That model configuration is the most natural for the calibration experiment because the GOCART DE scheme was designed to operate with the GOCART AP scheme, and so no intersectional redistribution of dust mass is performed, as it would be the case with MOSAIC or MADE.

At this point, it is pertinent to highlight that this study focuses on mineral dust and so it is the only aerosol specie for which emission is enabled (using the GOCART DE scheme). Nonetheless, and conversely to MOSAIC and MADE, the GOCART AP scheme initializes other aerosol species—typically urban, such as sulphates and black carbon, among others—to small non-zero amounts. This has a negligible impact on AOD, specially during the ADO event, but not so on AE, as it will be discussed later on in Section 3.3.

The evaluation of the WRF-chem's total-column dust load (in μm^3/μm^2) is as follows:

$$L_d = \sum_k \left(\sum_i \frac{\chi_{k,i}}{\rho_{d,i}} \right) \rho_{a,k} \Delta z_k \quad (3)$$

where $\chi_{k,i}$ is the dust mixing ratio (in kg_{dust}/kg_{air}) for the i-th dust section at the k-th model vertical layer, $\rho_{d,i}$ is the dust density (in kg_{dust}/m^3) for the i-th dust section, and $\rho_{a,k}$ and Δz_k are the air density (in kg_{air}/m^3) and the thickness (in m) of the k-th model vertical layer. The dust mixing ratios are the variables *DUST_i* for GOCART, *oin_a0i* for MOSAIC and *p25i*, *p25j* and *soila* for MADE. Although the dust diameter ranges observed in AERONET (0.1–30 μm) and simulated by WRF-chem differ (0.2–20 μm with GOCART and 0.037–10 μm with MOSAIC), observed dust particles in AERONET with diameters larger than 20 μm show a negligible concentration, lower than 1% of the total dust load, based on our own analysis of AERONET Level 1.5 inversion measurements available for this event at Granada. Indeed, the average concentration for dust particles with diameters in the range 10–20 μm during the event is below 5%.

The WRF-chem's output provides AOD at 400, 500, 600 and 1000 nm at every grid cell. Each of them, conveniently integrated for each grid column, makes up the total-column AOD at the corresponding wavelength. To precisely match the AERONET observing wavelengths, the Ångström turbidity coefficient, β, and the AE, α, are evaluated from a linear fit of the total-column spectral AODs using a log-log form of the Ångström's formula (Ångström, 1929). Then, those β and α values, combined with the Ångström's formula are used to evaluate the WRF-chem AOD at the AERONET wavelengths: 440, 675 and 870 nm.

Interestingly, while validating the β and α predicted by the MADE AP scheme, suspiciously large underestimations of the former and overestimations of the latter (as it will be shown later in Fig. 9), led us to notice that dust was not being properly accounted for by MADE during the Mie scattering calculations. In particular, the coarse dust contribution was omitted (possibly unintentionally) in the model's code while preparing the inputs for the Mie scattering routine in the function *optical_prep_modal* of *module_optical_averaging.F*. To solve it, the code was updated to include the factor "*mass_soil*xmas_sectc(isize)*" in the calculation of the variable *mass_oin*. This bug has probably been overlooked previously because it does not affect the dust size distribution and, typically, only AOD at some wavelength, but not α, is considered in the model's evaluation.

The spectral attenuated backscatter, β_λ^{att}, which is required for the comparison against the observed atmospheric profiles retrieved at 1064 nm from the E-PROFILE's ceilometer, is evaluated as (Mattis and Wagner, 2014):

$$\beta_\lambda^{att} = b_\lambda T_\lambda \tag{4}$$

where b_λ is the spectral backscatter coefficient and T_λ is the spectral attenuation of the emitted laser light on its way from the emitter to the scattering volume and from that volume back to the receiver.

WRF-chem provides the total backscatter extinction coefficient at 300, 500 and 1060 nm, i.e. the backscatter extinction integrated for all angles. To obtain the backscatter coefficient, b_λ, in units of *1/(L·sr)* (where *L* denotes an arbitrary length measure) WRF-chem's outputs must be divided by the so-called *lidar ratio* (known also to as extinction-to-backscatter ratio). Although it varies with wavelength and height, its value is typically assumed constant for each wavelength. In particular, for 355 and 532 nm, the lidar ratio values considered here are 52 ± 7 and 53 ± 6 sr, respectively (Fernández et al., 2019), while for 1064 nm, the considered ratio is 50 sr (Cazorla et al., 2017). From the backscattering coefficients determined at the WRF-chem wavelengths, the values at 355, 532 and 1064 nm are evaluated at each grid cell assuming that b_λ verifies the Ångström's formula, analogously to AOD.

The light attenuation for a scattering volume situated at vertical distance *r* from the ceilometer is evaluated as:

$$T_\lambda = \exp\left(-2\int_0^r \tau_\lambda dl\right) \tag{5}$$

where τ_λ is the extinction coefficient at wavelength λ. WRF-chem provides this coefficient at exactly the same wavelengths as AOD. From them, it is evaluated at 1064 nm, at every grid cell, using the Ångström's formula, analogously to AOD. The integral for every grid layer is evaluated as the sum of all extinction coefficients below times the thickness of their model layers.

3. Results

3.1. Calibration of the GOCART DE scheme

An increase (decrease) of *c* yields an increase (decrease) of the total dust load, as shown in Fig. 4. Also, the total dust load in Granada, which is located at 680 m a.s.l., is slightly higher, in general, than at Cerro Poyos, which is located at 1809 m a.s.l., for both the AERONET observations and the WRF-chem simulations. In particular, L_d shows a remarkable linear dependence against *c* (Fig. 5a).

The calibration of the GOCART DE scheme aims at adjusting the value of the *c* parameter to minimize the WRF-chem's L_d mean square error (MSE) at the two AERONET stations combined. To do so, the MSE is modeled as a quadratic polynomial of *c* (Fig. 5b), which is found to have the minimum at 0.57, slightly lower than the recommended value of 0.65. This local optimal value for *c* probes that the recommended value of 0.65 is not necessary the best at any immission region, as it also suggests that 0.57 might not be the best for other events or locations. Longer-term simulations would be needed to assert the validity of the recommend value for *c* (i.e., 0.65) or rather suggest a different one.

In absence of indirect aerosol effects, as in this summer 2021 ADO, it is expected that the linear trend revealed by Fig. 5a also holds for MOSAIC and MADE because, here, all the AP schemes share the same DE scheme. This allows estimating the optimal *c* values for both MOSAIC and MADE based on their relative differences at predicting L_d with respect to GOCART. In particular, MOSAIC produces a mean total dust load which is 4% smaller than that of GOCART, while the mean value predicted by MADE is 22% higher. Based on these results, the optimal *c* value for MOSAIC is set also to 0.57 (considering negligible the 4% difference against GOCART), while it is set to 0.45 for MADE.

With the optimal values of the *c* parameter for each AP scheme, Fig. 6 shows the simulated and observed L_d time series during the ADO event at the AERONET station in Granada.

3.2. Dust size distribution

Fig. 7 shows the average dust volume size distribution observed at the AERONET station in Granada against those simulated by the

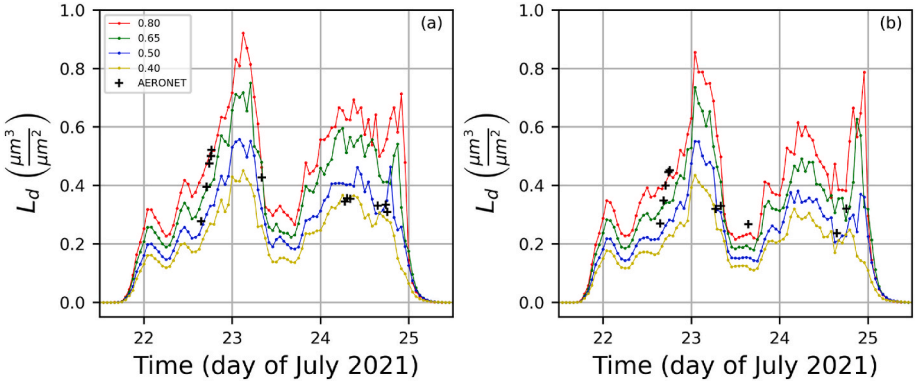

Fig. 4. Observed and modeled total dust load at the AERONET stations in Granada (a) and Cerro Poyos (b) for the GOCART DE scheme with the *c* parameter prescribed to 0.40 (yellow), 0.50 (blue), 0.65 (green) and 0.80 (red). The units of *c* are μg s^2 m^{-5} = $1e^{-9}$ kg s^2 m^{-5}.

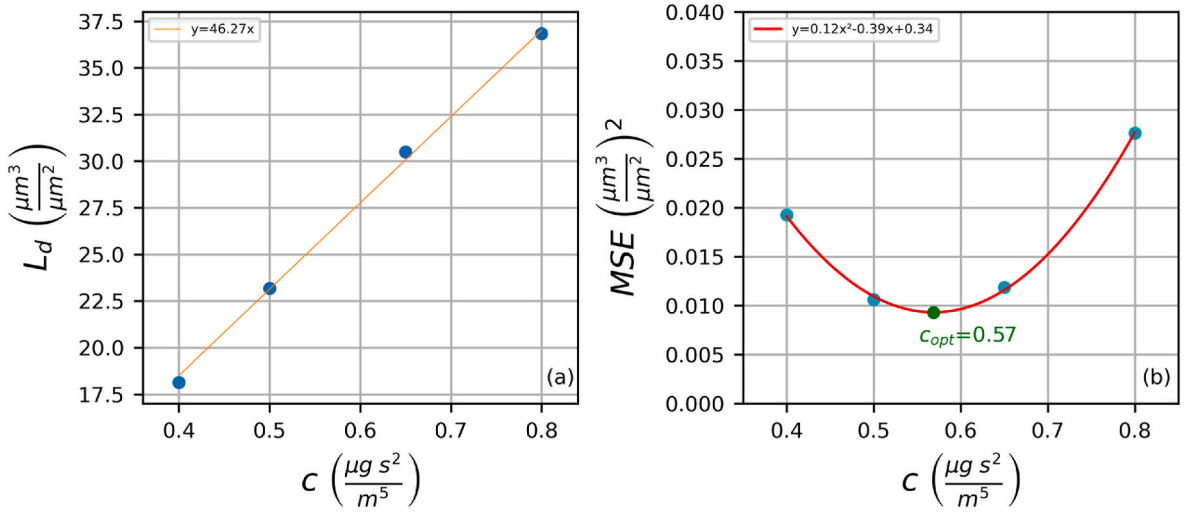

Fig. 5. Total dust load vs. GOCART DE scheme's c parameter at the two AERONET station locations combined. (a) Simulated mean total dust load against the c parameter and linear fit. (b) Total dust load MSE against the c parameter and 2-nd order polynomial fit.

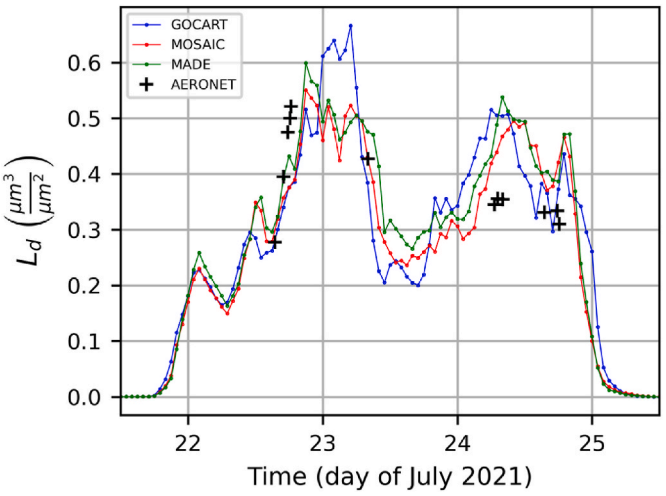

Fig. 6. Simulated and observed total dust at the AERONET station in Granada.

GOCART (Fig. 7a), MOSAIC (Fig. 7b) and MADE (Fig. 7c) AP schemes. The differences between the simulated and observed distributions for MOSAIC and MADE are remarkable and, as shown in Section 3.3, this has an important impact on the simulation of dust optical depth.

Although the observed size distribution clearly evidences the coarse dust mode, with modal value at about 3.5 μm, this is not so with the simulated size distributions by MOSAIC and MADE. Nonetheless, GOCART reproduces the observed coarse mode more consistently and, approximately, at the observed modal radius. MOSAIC underestimates the load of particles with sub-micron diameters and overestimates that of particles with diameter beyond ≈5 μm, which results in a blurring of the dust coarse mode, and an overestimation of its modal radius. Conversely, MADE largely overestimates the sub-micron particles while underestimates the load of particles with diameter beyond ≈3 μm. As a result, the dust coarse mode appears shifted towards too small radii.

3.3. Aerosol optical depth

All AP schemes show a temporal pattern which is consistent with that of the observed AOD (Fig. 8), thus supporting the hypothesis that dust is the dominant aerosol species during the ADO event. Nevertheless, and

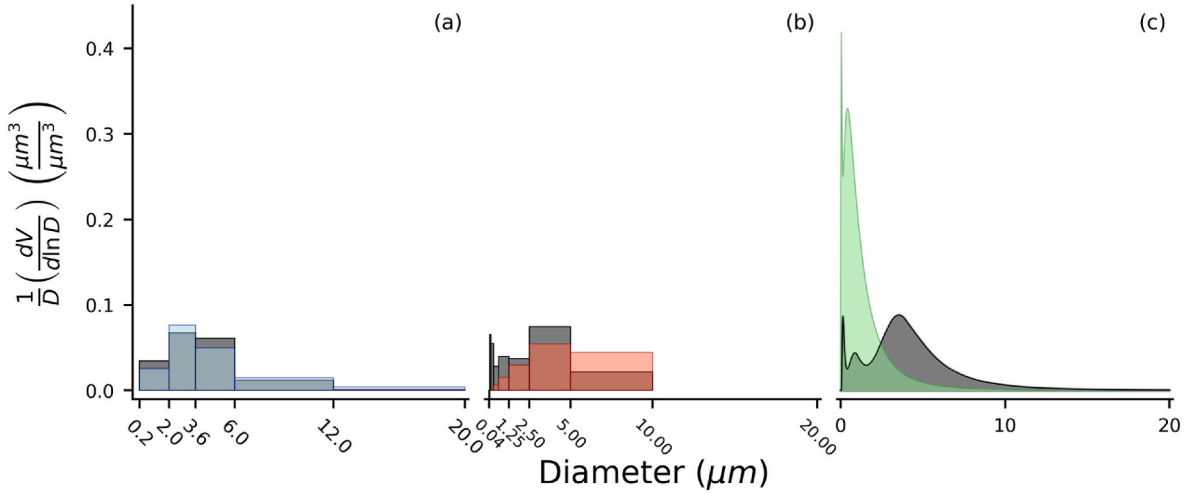

Fig. 7. Mean dust volume size distribution observed at the AERONET station in Granada (gray) and simulated with the GOCART (a), MOSAIC (b) and MADE (c) AP schemes during the ADO event. The observed volume size distribution, sampled at 22 particle diameters, is interpolated using quadratic splines and, for GOCART and MOSAIC, integrated throughout each section.

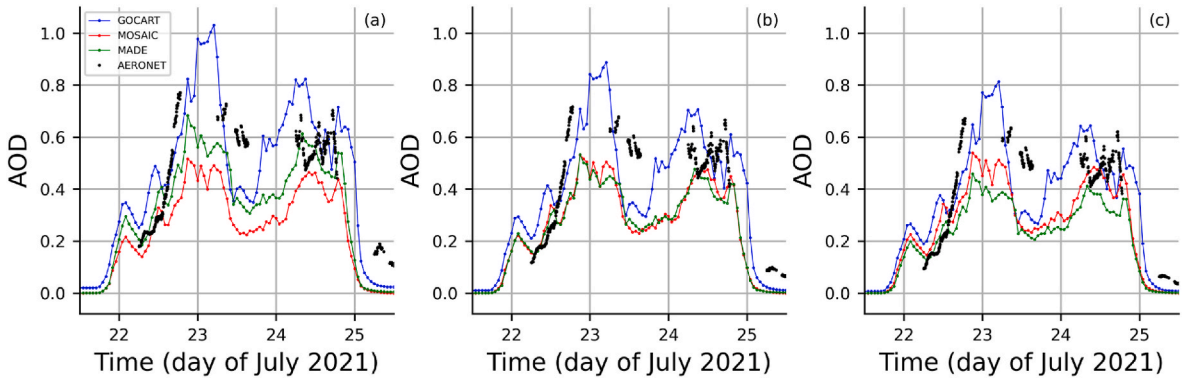

Fig. 8. Simulated AOD during the ADO event with the three AP schemes and observed values at the AERONET station in Granada at (a) 440 nm, (b) 675 nm and (c) 870 nm. The simulated values have been obtained from the original 300, 400, 600 and 1000 nm predictions and their associated AE using the Ångström's formula.

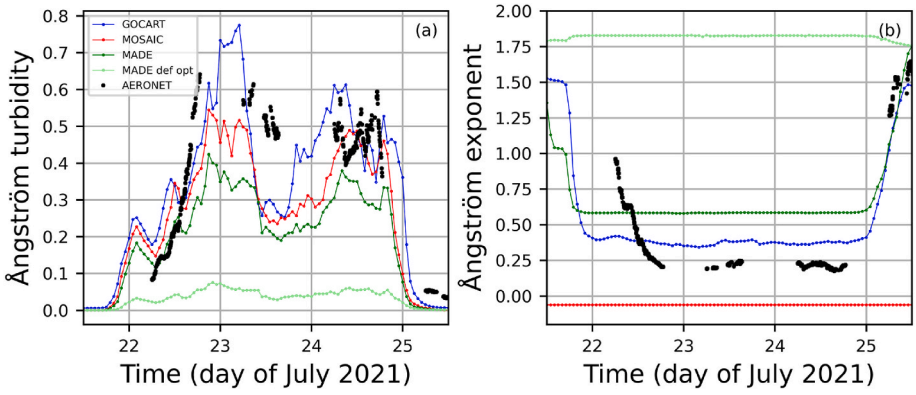

Fig. 9. Ångström's aerosol parameters, β (a) and α (b), during the ADO event for the AERONET observations and the three AP schemes. The plots for AE clearly show that WRF-chem anticipates the entry of the dust plume in the IP about 12 h with respect to the observed values. MADE def opt stands for the results using MADE before updating the code to include the coarse dust contribution, as described in Section 2.5.

conversely to MOSAIC and MADE, GOCART considers a default initial concentration of some aerosol species that are typically urban aerosols (e.g., sulphates and black carbon), whose impact on AOD is negligible compared to the dust optical depth during the ADO, but that has an important impact on AE as it will be shown later on. This is noticeable at the beginning and end of the GOCART AOD simulating results when compared to the other AP schemes results, especially at lower wavelengths (Fig. 8).

AOD at 440, 675 and 870 nm are reasonably well reproduced by GOCART during the ADO event, but they are clearly underestimated when using MADE and MOSAIC. The latter, in particular, presents similar AOD values for all wavelengths, i.e., a flat spectral response, which is totally unexpected. This inconsistency is directly related to the issues of the AP schemes at representing the aerosol size distribution (Fig. 7).

Alternatively, the skill of the AP schemes at predicting both the AOD magnitude and its spectral response can be investigated by the evaluation of β and α, respectively, as shown in Fig. 9. AE is extremely sensitive to the aerosol size distribution for sub-micron aerosol particles. Hence, the presence of background aerosols in GOCART is deemed determinant for its higher performance in the evaluation of AE.

Overall, GOCART performs best for both the AOD magnitude (Fig. 9a) and its spectral variation (Fig. 9b). In particular, the GOCART's default background aerosols appear effective to model the spectral variation of AOD, i.e., the value of AE. MOSAIC does not count with such background aerosols, contributing to the extremely low AE value shown in Fig. 9b. In addition, MOSAIC's AE value stays constant throughout the entire simulation, which suggests that the shape of the aerosol size distribution remains unaltered when using MOSAIC. In this respect, Fig. 10 shows the relative L_d ratios between consecutive sections for both GOCART (which provides a reasonable evaluation of AE) and MOSAIC. Conversely to GOCART, the L_d ratios in MOSAIC remain constant and ≈1 virtually always, which confirms the highly unlikely situation of having a constant shape for the aerosol size distribution throughout the entire simulation.

Overall, these AE results for MOSAIC point towards a coupling issue between the GOCART DE scheme and the MOSAIC AP scheme. The dust emission flux in the GOCART DE scheme is different for each particle size because the wind threshold in Eq. (1) has a non-linear dependency on the particle's diameter and the soil moisture (Ginoux et al., 2001; Marticorena and Bergametti, 1995). When coupled to the GOCART AP scheme, the dust size distribution can change over time (Fig. 10a) because the dust emission flux is evaluated independently for each model's dust section. However, to couple the DE scheme with the MOSAIC AP scheme, the dust flux is first aggregated over the five GOCART sections and then it is redistributed over the eight MOSAIC sections, relying on a set of prescribed constant weights that represent the fraction of emitted dust in each section. Therefore, although the total dust load in MOSAIC may change throughout time, the shape of the dust size distribution is not allowed to do so by construction. Although the modal approach of MADE appears more consistent than MOSAIC in terms of spectral dependence, the high values of α indicate an underestimation of the size of coarse particles, in agreement with Fig. 7, which explains the poor representation of the AOD magnitude for the longer wavelengths.

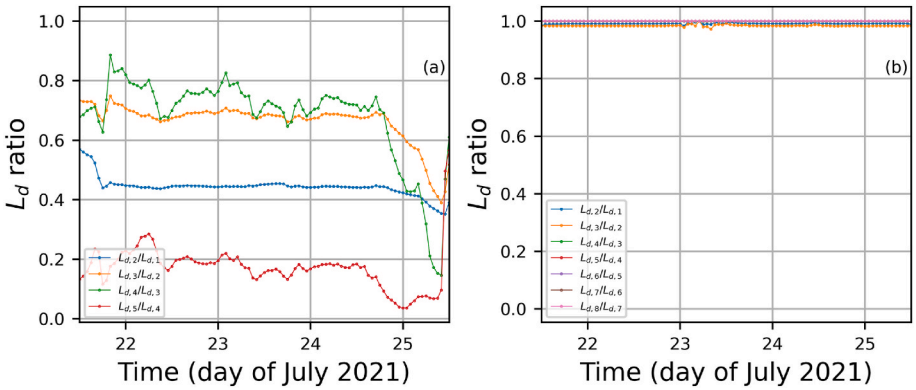

Fig. 10. Relative fraction of dust particles between consecutive sections of GOCART (a) and MOSAIC (b). The legend shows the ordinal numbers of each section. See Table 1 for the particle size limits of each section.

3.4. Dust vertical profile

The vertical distribution of dust in the atmosphere can be indirectly inferred from the backscattering profile observed from the ceilometer and lidar instruments (Section 2.2). Here, the observed backscattering profiles are compared to the simulated ones using the *attenuated backscatter* in the case of the ceilometer, which is evaluated in WRF-chem as described in Section 2.5, and the *backscatter* in the case of the lidar.

Fig. 11 compares the ceilometric data against the WRF-chem simulations. Overall, all AP schemes yield attenuated backscatter values notably below the observed ones. Among the models, GOCART yields the thickest dust layer, in accordance with the AOD results presented in Section 3.3. Overall, WRF-chem appears to reproduce the dust entrance approximately at the right altitude, mostly below 3 km, regardless the AP choice.

Similar conclusions are apparent in Fig. 12, that compares the backscatter coefficient retrieved from the MULHACEN lidar against the WRF-chem predictions. While the lidar observations are more reliable than those of the ceilometer, the lidar cannot operate continuously, thus the gaps in the observations. Now, the model's attenuated backscatter agrees better with the observed values than in Fig. 11, although still with significant model−observation differences, consistently with other studies (Saidou Chaibou et al., 2020a; Teixeira et al., 2016).

Alternatively to the previous comparisons, the vertical distribution of dust can be inferred by a series of vertical profiles as in Fig. 13.

As in Figs. 11 and 12, a generally lower backscatter is always observed except at 22/07 14:00, where MADE presents a pronounced peak. Also, although WRF-chem's predictions show a smoother vertical variability in terms of dust concentration, the height of the most important layers is predicted reasonably well. Remarkably, MADE presents greater backscatter at 355 nm, in agreement with the greater concentration of small dust particles observed in the distribution of Fig. 7. Likewise, the opposite trend is observed for MOSAIC.

4. Conclusions

This study benchmarks three of the most widely used aerosol schemes in WRF-chem, namely, GOCART, MOSAIC and MADE, during a strong and dry Saharan dust intrusion event in southern IP. All schemes use different approaches to parameterize aerosols and, in particular, to parameterize dust. After a proper calibration of the DE scheme, which is common for the three AP schemes, the three aerosol schemes perform similarly in terms of both extent and variability of the event, and in the total dust loading, with differences between models below 4%. The most important discrepancies concern the dust optical properties and are due to reasons that include differences in the dust treatment, the presence of background aerosols and the parameterization of optical properties.

It has been found that the redistribution of the dust emitted by the DE scheme to the MOSAIC sections and the MADE modes does not allow a proper evolution of dust over the different sections, or modes, and produces an invariant shape of the dust size distribution. In addition, MOSAIC and MADE demonstrated deficiencies to represent the actual dust size distribution that led to an incorrect prediction of AE. Accounting for background aerosols, even if they are prescribed in a very low concentration, as done by GOCART, is beneficial, especially for AE.

The parameterization of aerosol optical properties is complex and involves redistributions of various aerosol properties between different sections and modes back and forth. However, small variations in the

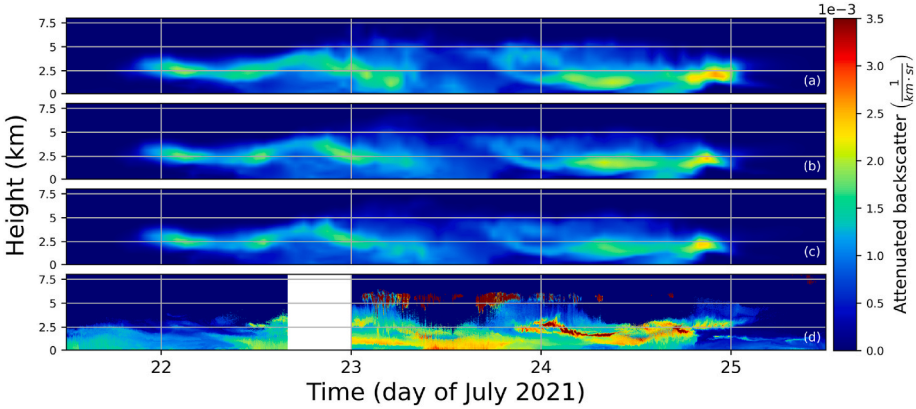

Fig. 11. Attenuated backscatter at 1064 nm simulated using the GOCART (a), MOSAIC (b) and MADE (c) WRF-chem's AP schemes, and the values measured by the ceilometer (d) at Granada. The red patches at around 6 km in the observed values correspond to small cloud structures aloft the dust layer.

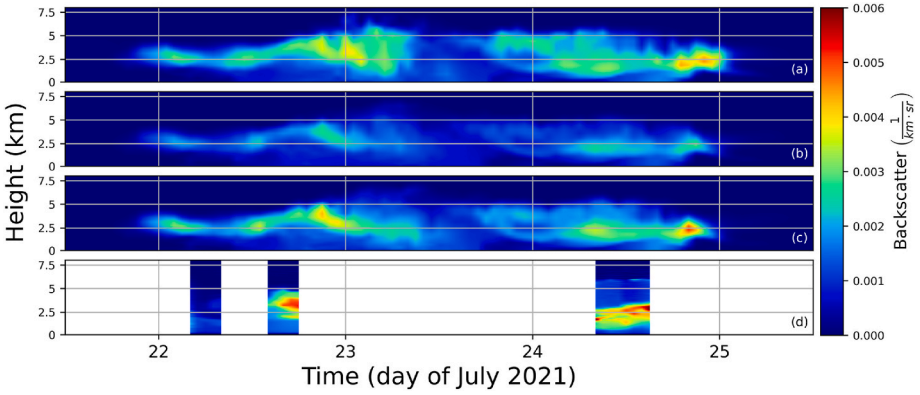

Fig. 12. As Fig. 11 but for the lidar observations at 532 nm.

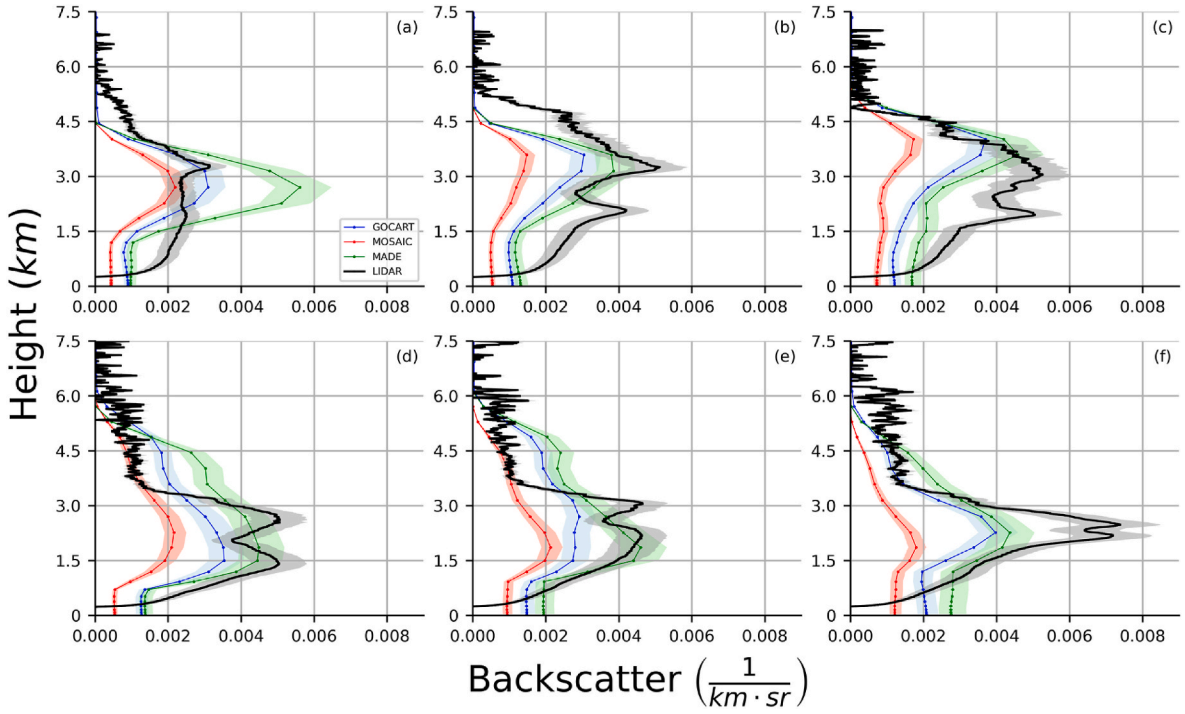

Fig. 13. Vertical profiles of backscatter at 355 nm retrieved from MULHACEN lidar at (a) 07/22 14:00, (b) 07/22 16:00, (c) 07/22 18:00, (d) 07/24 12:00, (e) 07/24 14:00, (f) 07/24 17:00. The shaded areas represent the uncertainties of 15% in the case of lidar data and the originated due to the lidar ratio uncertainty at 355 nm (Sections 2.2 and 2.5).

redistribution weights can have notable impacts in the results. In addition, various issues were found in the model's code. Some, such as the lack of coarse mineral dust in MADE, have been corrected for this work. Others will be addressed in a future studies.

Overall, GOCART proved the most accurate and runs faster than MOSAIC and MADE. Hence, altogether, GOCART appears a generally better choice for strong and dry ADO events in southern IP. However, it is important to remark that this choice is heavily influenced by the necessities of the application. A subsequent study is ongoing to study the accuracy of the GOCART AP scheme during a wet dust outbreak in the same study region.

CRediT authorship contribution statement

Miguel Pino-Carmona: Writing – review & editing, Writing – original draft, Software, Methodology, Investigation, Data curation, Conceptualization. **José A. Ruiz-Arias:** Writing – review & editing, Writing – original draft, Supervision, Resources, Project administration, Investigation, Conceptualization. **Sol Fernández-Carvelo:** Data curation. **Juan A. Bravo-Aranda:** Data curation. **Lucas Alados-Arboledas:** Writing – review & editing, Supervision, Resources, Project administration.

Data availability

Data are freely available in the official sites indicated in Section 2.2.

Declaration of competing interest

The authors declare that they have no known competing financial interests or personal relationships that could have appeared to influence the work reported in this paper.

Acknowledgments

The work is funded by the Office of Knowledge, Research and

University of Junta de Andalucia through the project AEROPRE (P-18-RT-3820). This work received support also from the European Union's Horizon 2020 research and innovation program through projects ACTRIS.IMP (grant agreement No 871115) and ATMO_ACCESS (grant agreement No 101008004), by the Spanish Ministry of Science and Innovation through projects ELPIS PID2020-120015RB-I00 MCIN/AEI/10.13039/501100011033 and ACTRIS-España RED2022-134824-E and by University of Granada Plan Propio through Singular Laboratory program (AGORA, LS2022-1) and Unidad Científica de Excelencia program (Sistema Tierra, UCE-PP2017-2). The authors thankfully acknowledge the computer resources, technical expertise and assistance provided by the SCBI (Supercomputing and Bioinformatics) center of the University of Malaga.

Data availability

Data will be made available on request.

References

Ackermann, I.J., Hass, H., Memmesheimer, M., Ebel, A., Binkowski, F.S., Shankar, U., 1998. Modal aerosol dynamics model for Europe. Atmos. Environ. 32, 2981–2999. https://doi.org/10.1016/S1352-2310(98)00006-5.

Alados-Arboledas, L., Müller, D., Guerrero-Rascado, J.L., Navas-Guzmán, F., Pérez-Ramírez, D., Olmo, F.J., 2011. Optical and microphysical properties of fresh biomass burning aerosol retrieved by Raman lidar, and star-and sun-photometry: remote sensing of fresh BB aerosol. Geophys. Res. Lett. 38. https://doi.org/10.1029/2010GL045999 n/a-n/a.

Albrecht, B.A., 1989. Aerosols, cloud microphysics, and fractional cloudiness. Science 245, 1227–1230. https://doi.org/10.1126/science.245.4923.1227.

Amiri-Farahani, A., Allen, R.J., Li, K., Chu, J., 2019. The semidirect effect of combined dust and sea salt aerosols in a multimodel analysis. Geophys. Res. Lett. 46, 10512–10521. https://doi.org/10.1029/2019GL084590.

Ångström, A., 1929. On the atmospheric transmission of sun radiation and on dust in the air. Geogr. Ann. 11, 156–166. https://doi.org/10.2307/519399.

Bègue, N., Tulet, P., Pelon, J., Aouizerats, B., Berger, A., Schwarzenboeck, A., 2015. Aerosol processing and CCN formation of an intense Saharan dust plume during the EUCAARI 2008 campaign. Atmos. Chem. Phys. 15, 3497–3516. https://doi.org/10.5194/acp-15-3497-2015.

Bellouin, N., Boucher, O., Haywood, J., Reddy, M.S., 2005. Global estimate of aerosol direct radiative forcing from satellite measurements. Nature 438, 1138–1141. https://doi.org/10.1038/nature04348.

Bran, S.H., Macatangay, R., Surapipith, V., Chotamonsak, C., Chantara, S., Han, Z., Li, J., 2022. Surface PM2.5 mass concentrations during the dry season over northern Thailand: sensitivity to model aerosol chemical schemes and the effects on regional meteorology. Atmos. Res. 277, 106303. https://doi.org/10.1016/j.atmosres.2022.106303.

Bucaram, C.J., Bowman, F.M., 2021. WRF-chem modeling of summertime air pollution in the northern great plains: chemistry and aerosol mechanism intercomparison. Atmosphere 12, 1121. https://doi.org/10.3390/atmos12091121.

Casquero-Vera, J.A., Pérez-Ramírez, D., Lyamani, H., Rejano, F., Casans, A., Titos, G., Olmo, F.J., Dada, L., Hakala, S., Hussein, T., Lehtipalo, K., Paasonen, P., Hyvärinen, A., Pérez, N., Querol, X., Rodríguez, S., Kalivitis, N., González, Y., Alghamdi, M.A., Kerminen, V.-M., Alastuey, A., Petäjä, T., Alados-Arboledas, L., 2023. Impact of desert dust on new particle formation events and the cloud condensation nuclei budget in dust-influenced areas. Atmos. Chem. Phys. 23 (24), 15795–15814.

Cazorla, A., Casquero-Vera, J.A., Román, R., Guerrero-Rascado, J.L., Toledano, C., Cachorro, V.E., Orza, J.A.G., Cancillo, M.L., Serrano, A., Titos, G., Pandolfi, M., Alastuey, A., Hanrieder, N., Alados-Arboledas, L., 2017. Near-real-time processing of a ceilometer network assisted with sun-photometer data: monitoring a dust outbreak over the Iberian Peninsula. Atmos. Chem. Phys. 17, 11861–11876. https://doi.org/10.5194/acp-17-11861-2017.

Chin, M., Rood, R.B., Lin, S., Müller, J., Thompson, A.M., 2000. Atmospheric sulfur cycle simulated in the global model GOCART: model description and global properties. J. Geophys. Res. 105, 24671–24687. https://doi.org/10.1029/2000JD900384.

Díaz, J., Linares, C., Carmona, R., Russo, A., Ortiz, C., Salvador, P., Trigo, R.M., 2017. Saharan dust intrusions in Spain: health impacts and associated synoptic conditions. Environ. Res. 156, 455–467. https://doi.org/10.1016/j.envres.2017.03.047.

Eltahan, M., Shokr, M., Sherif, A., 2018. Simulation of severe dust events over Egypt using tuned dust schemes in weather research forecast (WRF-Chem). Atmosphere 9, 246. https://doi.org/10.3390/atmos9070246.

Esmaeil, N., Gharagozloo, M., Rezaei, A., Grunig, G., 2014. Dust events, pulmonary diseases and immune system. Afr. J. Clin. Exp. Immunol. 3, 20–29.

Fast, J.D., Gustafson, W.I., Easter, R.C., Zaveri, R.A., Barnard, J.C., Chapman, E.G., Grell, G.A., Peckham, S.E., 2006. Evolution of ozone, particulates, and aerosol direct radiative forcing in the vicinity of Houston using a fully coupled meteorology-chemistry-aerosol model. J. Geophys. Res. 111, 2005JD006721. https://doi.org/10.1029/2005JD006721.

Fernández, A.J., Sicard, M., Costa, M.J., Guerrero-Rascado, J.L., Gómez-Amo, J.L., Molero, F., Barragán, R., Basart, S., Bortoli, D., Bedoya-Velásquez, A.E., Utrillas, M. P., Salvador, P., Granados-Muñoz, M.J., Potes, M., Ortiz-Amezcua, P., Martínez-Lozano, J.A., Artíñano, B., Muñoz-Porcar, C., Salgado, R., Román, R., Rocadenbosch, F., Salgueiro, V., Benavent-Oltra, J.A., Rodríguez-Gómez, A., Alados-Arboledas, L., Comerón, A., Pujadas, M., 2019. Extreme, wintertime Saharan dust intrusion in the Iberian Peninsula: lidar monitoring and evaluation of dust forecast models during the February 2017 event. Atmos. Res. 228, 223–241. https://doi.org/10.1016/j.atmosres.2019.06.007.

Georgiou, G.K., Christoudias, T., Proestos, Y., Kushta, J., Hadjinicolaou, P., Lelieveld, J., 2018. Air quality modelling in the summer over the eastern Mediterranean using WRF-Chem: chemistry and aerosol mechanism intercomparison. Atmos. Chem. Phys. 18, 1555–1571. https://doi.org/10.5194/acp-18-1555-2018.

Giles, D.M., Sinyuk, A., Sorokin, M.G., Schafer, J.S., Smirnov, A., Slutsker, I., Eck, T.F., Holben, B.N., Lewis, J.R., Campbell, J.R., others, 2019. Advancements in the Aerosol Robotic Network (AERONET) Version 3 database–automated near-real-time quality control algorithm with improved cloud screening for Sun photometer aerosol optical depth (AOD) measurements. Atmos. Meas. Tech. 12, 169–209. https://doi.org/10.5194/amt-12-169-2019.

Ginoux, P., Chin, M., Tegen, I., Prospero, J.M., Holben, B., Dubovik, O., Lin, S., 2001. Sources and distributions of dust aerosols simulated with the GOCART model. J. Geophys. Res. 106, 20255–20273. https://doi.org/10.1029/2000JD000053.

Granados-Muñoz, M.J., Benavent-Oltra, J.A., Pérez-Ramírez, D., Lyamani, H., Guerrero-Rascado, J.L., Bravo-Aranda, J.A., Navas-Guzmán, F., Valenzuela, A., Olmo, F.J., Alados-Arboledas, L., 2020. Evaluation of LIRIC algorithm performance using independent sun-sky photometer data at two altitude levels. Rem. Sens. 12 (5), 842. https://doi.org/10.3390/rs12050842 art. no.

Grell, G.A., Peckham, S.E., Schmitz, R., McKeen, S.A., Frost, G., Skamarock, W.C., Eder, B., 2005. Fully coupled "online" chemistry within the WRF model. Atmos. Environ. 39, 6957–6975. https://doi.org/10.1016/j.atmosenv.2005.04.027.

Guerrero-Rascado, J.L., Olmo, F.J., Avilés-Rodríguez, I., Navas-Guzmán, F., Pérez-Ramírez, D., Lyamani, H., Alados Arboledas, L., 2009. Extreme Saharan dust event over the southern Iberian Peninsula in september 2007: active and passive remote sensing from surface and satellite. Atmos. Chem. Phys. 9, 8453–8469. https://doi.org/10.5194/acp-9-8453-2009.

Guerrero-Rascado, J.L., Ruiz, B., Aladosarboledas, L., 2008. Multi-spectral Lidar characterization of the vertical structure of Saharan dust aerosol over southern Spain. Atmos. Environ. 42, 2668–2681. https://doi.org/10.1016/j.atmosenv.2007.12.062.

Gueye, M., Jenkins, G.S., 2019. Investigating the sensitivity of the WRF-Chem horizontal grid spacing on P M 10 concentration during 2012 over West Africa. Atmos. Environ. 196, 152–163. https://doi.org/10.1016/j.atmosenv.2018.09.064.

Hersbach, H., Bell, B., Berrisford, P., Hirahara, S., Horányi, A., Muñoz-Sabater, J., Nicolas, J., Peubey, C., Radu, R., Schepers, D., Simmons, A., Soci, C., Abdalla, S., Abellan, X., Balsamo, G., Bechtold, P., Biavati, G., Bidlot, J., Bonavita, M., Chiara, G., Dahlgren, P., Dee, D., Diamantakis, M., Dragani, R., Flemming, J., Forbes, R., Fuentes, M., Geer, A., Haimberger, L., Healy, S., Hogan, R.J., Hólm, E., Janisková, M., Keeley, S., Laloyaux, P., Lopez, P., Lupu, C., Radnoti, G., Rosnay, P., Rozum, I., Vamborg, F., Villaume, S., Thépaut, J., 2020. The ERA5 global reanalysis. Q. J. R. Meteorol. Soc. 146, 1999–2049. https://doi.org/10.1002/qj.3803.

Huneeus, N., Schulz, M., Balkanski, Y., Griesfeller, J., Prospero, J., Kinne, S., Bauer, S., Boucher, O., Chin, M., Dentener, F., Diehl, T., Easter, R., Fillmore, D., Ghan, S., Ginoux, P., Grini, A., Horowitz, L., Koch, D., Krol, M.C., Landing, W., Liu, X., Mahowald, N., Miller, R., Morcrette, J.-J., Myhre, G., Penner, J., Perlwitz, J., Stier, P., Takemura, T., Zender, C.S., 2011. Global dust model intercomparison in AeroCom phase I. Atmos. Chem. Phys. 11, 7781–7816. https://doi.org/10.5194/acp-11-7781-2011.

Intergovernmental Panel On Climate Change, 2023. Climate Change 2021 – the Physical Science Basis: Working Group I Contribution to the Sixth Assessment Report of the Intergovernmental Panel on Climate Change, first ed. Cambridge University Press. https://doi.org/10.1017/9781009157896.

Jenkins, G., Gueye, M., 2022. Annual and early summer variability in WRF-CHEM simulated West African PM10 during 1960–2016. Atmos. Environ. 273, 118957. https://doi.org/10.1016/j.atmosenv.2022.118957.

Karydis, V.A., Kumar, P., Barahona, D., Sokolik, I.N., Nenes, A., 2011. On the effect of dust particles on global cloud condensation nuclei and cloud droplet number. J. Geophys. Res. 116, D23204. https://doi.org/10.1029/2011JD016283.

Kazem, A.A., Chaichan, M.T., Kazem, H.A., 2014. Dust effect on photovoltaic utilization in Iraq: review article. Renew. Sustain. Energy Rev. 37, 734–749. https://doi.org/10.1016/j.rser.2014.05.073.

Knippertz, P., Stuut, J.-B.W. (Eds.), 2014. Mineral Dust: A Key Player in the Earth System. Springer, Netherlands, Dordrecht. https://doi.org/10.1007/978-94-017-8978-3.

Laj, P., Myhre, C.L., Riffault, V., Amiridis, V., Fuchs, H., Eleftheriadis, K., Petäjä, T., Kivekäs, N., Juurola, E., Saponaro, G., Philippin, S., Cornacchia, C., Alados Arboledas, L., Baars, H., Claude, A., De Mazière, M., Dils, B., Dufresne, M., Evangeliou, N., Favez, O., Fiebig, M., Haeffelin, M., Herrmann, H., Höhler, K., Illmann, N., Kreuter, A., Ludewig, E., Engelmann, R., Wehrle, G., Belegante, L., Flentje, H., Wandinger, U., Bais, A., Komppula, M., Lehtinen, K.E.J., Mona, L., Murberg, L.E., Nicolae, D., Novelli, A., O'Connor, E., Ohneiser, K., Petracca Altieri, R.M., Picquet-Varrault, B., van Pinxteren, D., Pospichal, B., Putaud, J.-P., Reimann, S., Salameh, T., Siomos, N., Stachlewska, I., Tillmann, R., Voudouri, K.A., Wiedensohler, A., Apituley, A., Comerón, A., Gysel-Beer, M., Mihalopoulos, N., Nikolova, N., Pietruczuk, A., Sauvage, S., Sciare, J., Skov, H., Svendby, T., Swietlicki, E., Tonev, D., Vaughan, G., Zdimal, V., Baltensperger, U., Doussin, J.-F., Kulmala, M., Pappalardo, G., Sorvari Sundet, S., Vana, M., 2024. Aerosol, Clouds and

Trace Gases Research Infrastructure – ACTRIS, the European Research Infrastructure Supporting Atmospheric Science. Accepted for publication in the Bulletin of the American Meteorological Society.

LeGrand, S.L., Polashenski, C., Letcher, T.W., Creighton, G.A., Peckham, S.E., Cetola, J. D., 2019. The AFWA dust emission scheme for the GOCART aerosol model in WRF-Chem v3.8.1. Geosci. Model Dev. (GMD) 12, 131–166. https://doi.org/10.5194/gmd-12-131-2019.

Lohmann, U., Feichter, J., 2005. Global indirect aerosol effects: a review. Atmos. Chem. Phys. 5, 715–737. https://doi.org/10.5194/acp-5-715-2005.

Maghami, M.R., Hizam, H., Gomes, C., Radzi, M.A., Rezadad, M.I., Hajighorbani, S., 2016. Power loss due to soiling on solar panel: a review. Renew. Sustain. Energy Rev. 59, 1307–1316. https://doi.org/10.1016/j.rser.2016.01.044.

Mandija, F., Sicard, M., Comerón, A., Alados-Arboledas, L., Guerrero-Rascado, J.L., Barragan, R., Bravo-Aranda, J.A., Granados-Muñoz, M.J., Lyamani, H., Muñoz Porcar, C., Rocadenbosch, F., Rodríguez, A., Valenzuela, A., García Vizcaíno, D., 2017. Origin and pathways of the mineral dust transport to two Spanish EARLINET sites: effect on the observed columnar and range-resolved dust optical properties. Atmos. Res. 187, 69–83. https://doi.org/10.1016/j.atmosres.2016.12.002.

Marticorena, B., Bergametti, G., 1995. Modeling the atmospheric dust cycle: 1. Design of a soil-derived dust emission scheme. J. Geophys. Res. 100, 16415–16430. https://doi.org/10.1029/95JD00690.

Mattis, I., Wagner, F., 2014. E-PROFILE: glossary of lidar and ceilometer variables [WWW Document]. URL. https://www.eumetnet.eu/wp-content/uploads/2016/10/ALC_glossary.pdf.

Mesbahzadeh, T., Salajeghe, A., Sardoo, F.S., Zehtabian, G., Ranjbar, A., Marcello Miglietta, M., Karami, S., Krakauer, N.Y., 2020. Spatial-temporal variation characteristics of vertical dust flux simulated by WRF-chem model with GOCART and AFWA dust emission schemes (case study: central plateau of Iran). Appl. Sci. 10, 4536. https://doi.org/10.3390/app10134536.

Morichetti, M., Passerini, G., Virgili, S., Mancinelli, E., Rizza, U., 2020. A preliminary assessment of mineral dust outbreaks in Italian coastal cities. Int. J. EI 3, 132–142. https://doi.org/10.2495/EI-V3-N2-132-142.

Morrison, H., Curry, J.A., Khvorostyanov, V.I., 2005. A new double-moment microphysics parameterization for application in cloud and climate models. Part I: description. J. Atmos. Sci. 62, 1665–1677. https://doi.org/10.1175/JAS3446.1.

Nogueira, J., Evangelista, H., Valeriano, C.D.M., Sifeddine, A., Neto, C., Vaz, G., Moreira, L.S., Cordeiro, R.C., Turcq, B., Aniceto, K.C., Neto, A.B., Martins, G., Barbosa, C.G.G., Godoi, R.H.M., Shimizu, M.H., 2021. Dust arriving in the Amazon basin over the past 7,500 years came from diverse sources. Commun Earth Environ 2, 5. https://doi.org/10.1038/s43247-020-00071-w.

Ortiz-Amezcua, P., Guerrero-Rascado, J.L., Granados-Muñoz, M.J., Benavent-Oltra, J.A., Böckmann, C., Samaras, S., Stachlewska, I.S., Janicka, Ł., Baars, H., Bohlmann, S., Alados-Arboledas, L., 2017. Microphysical characterization of long-range transported biomass burning particles from North America at three EARLINET stations. Atmos. Chem. Phys. 17, 5931–5946. https://doi.org/10.5194/acp-17-5931-2017.

Palacios-Peña, L., Lorente-Plazas, R., Montávez, J.P., Jiménez-Guerrero, P., 2019. Saharan dust modeling over the Mediterranean Basin and central Europe: does the resolution matter? Front. Earth Sci. 7, 290. https://doi.org/10.3389/feart.2019.00290.

Pappalardo, G., Amodeo, A., Apituley, A., Comeron, A., Freudenthaler, V., Linné, H., Ansmann, A., Bösenberg, J., D'Amico, G., Mattis, I., Mona, L., Wandinger, U., Amiridis, V., Alados-Arboledas, L., Nicolae, D., Earlinet, Wiegner M., 2014. Towards an advanced sustainable European aerosol lidar network. Atmos. Meas. Tech. 7 (8), 2389–2409. https://doi.org/10.5194/amt-7-2389-2014.

Parajuli, S.P., Stenchikov, G.L., Ukhov, A., Kim, H., 2019. Dust emission modeling using a new high-resolution dust source function in WRF-chem with implications for air quality. JGR Atmospheres 124, 10109–10133. https://doi.org/10.1029/2019JD030248.

Patrón, D., Lyamani, H., Titos, G., Casquero-Vera, J.A., Cardell, C., Močnik, G., Alados-Arboledas, L., Olmo, F.J., 2017. Monumental heritage exposure to urban black carbon pollution. Atmos. Environ. 170, 22–32. https://doi.org/10.1016/j.atmosenv.2017.09.030.

Rizza, U., Avolio, E., Morichetti, M., Di Liberto, L., Bellini, A., Barnaba, F., Virgili, S., Passerini, G., Mancinelli, E., 2023. On the interplay between desert dust and meteorology based on WRF-chem simulations and remote sensing observations in the Mediterranean Basin. Rem. Sens. 15, 435. https://doi.org/10.3390/rs15020435.

Rizza, U., Miglietta, M.M., Mangia, C., Ielpo, P., Morichetti, M., Iachini, C., Virgili, S., Passerini, G., 2018. Sensitivity of WRF-Chem model to land surface schemes: assessment in a severe dust outbreak episode in the Central Mediterranean (Apulia Region). Atmos. Res. 201, 168–180. https://doi.org/10.1016/j.atmosres.2017.10.022.

Rizza, U., Barnaba, F., Miglietta, M.M., Mangia, C., Di Liberto, L., Dionisi, D., Costabile, F., Grasso, F., Gobbi, G.P., 2017. WRF-Chem model simulations of a dust outbreak over the central Mediterranean and comparison with multi-sensor desert dust observations. Atmos. Chem. Phys. 17, 93–115. https://doi.org/10.5194/acp-17-93-2017.

Rosenfeld, D., Rudich, Y., Lahav, R., 2001. Desert dust suppressing precipitation: a possible desertification feedback loop. Proc. Natl. Acad. Sci. U.S.A. 98, 5975–5980. https://doi.org/10.1073/pnas.101122798.

Russo, A., Sousa, P.M., Durão, R.M., Ramos, A.M., Salvador, P., Linares, C., Díaz, J., Trigo, R.M., 2020. Saharan dust intrusions in the Iberian Peninsula: predominant synoptic conditions. Sci. Total Environ. 717, 137041. https://doi.org/10.1016/j.scitotenv.2020.137041.

Ryder, C.L., Bézier, C., Dacre, H.F., Clarkson, R., Amiridis, V., Marinou, E., Proestakis, E., Kipling, Z., Benedetti, A., Parrington, M., Rémy, S., Vaughan, M., 2023. Aircraft engine dust ingestion at global airports (preprint). Atmospheric, Meteorological and Climatological Hazards. https://doi.org/10.5194/egusphere-2023-662.

Saidou Chaibou, A.A., Ma, X., Kumar, K.R., Jia, H., Tang, Y., Sha, T., 2020a. Evaluation of dust extinction and vertical profiles simulated by WRF-Chem with CALIPSO and AERONET over North Africa. J. Atmos. Sol. Terr. Phys. 199, 105213. https://doi.org/10.1016/j.jastp.2020.105213.

Saidou Chaibou, A.A., Ma, X., Sha, T., 2020b. Dust radiative forcing and its impact on surface energy budget over West Africa. Sci. Rep. 10, 12236. https://doi.org/10.1038/s41598-020-69223-4.

Salvador, P., Pey, J., Pérez, N., Querol, X., Artíñano, B., 2022. Increasing atmospheric dust transport towards the western Mediterranean over 1948–2020. npj Clim Atmos Sci 5, 34. https://doi.org/10.1038/s41612-022-00256-4.

Sinyuk, A., Holben, B.N., Eck, T.F., Giles, D.M., Slutsker, I., Korkin, S., Schafer, J.S., Smirnov, A., Sorokin, M., Lyapustin, A., 2020. The AERONET Version 3 aerosol retrieval algorithm, associated uncertainties and comparisons to Version 2 (preprint). Aerosols/Remote Sensing/Data Processing and Information Retrieval. https://doi.org/10.5194/amt-2019-474.

Soupiona, O., Samaras, S., Ortiz-Amezcua, P., Böckmann, C., Papayannis, A., Moreira, G. A., Benavent-Oltra, J.A., Guerrero-Rascado, J.L., Bedoya-Velásquez, A.E., Olmo, F.J., Román, R., Kokkalis, P., Mylonaki, M., Alados-Arboledas, L., Papanikolaou, C.A., Foskinis, R., 2019. Retrieval of optical and microphysical properties of transported Saharan dust over Athens and Granada based on multi-wavelength Raman lidar measurements: study of the mixing processes. Atmos. Environ. 214, 116824. https://doi.org/10.1016/j.atmosenv.2019.116824.

Su, L., Fung, J.C.H., 2018. Investigating the role of dust in ice nucleation within clouds and further effects on the regional weather system over East Asia – Part 1: model development and validation. Atmos. Chem. Phys. 18, 8707–8725. https://doi.org/10.5194/acp-18-8707-2018.

Tao, W.-K., Chern, J., Iguchi, T., Lang, S., Lee, M.-I., Li, X., Loftus, A., Matsui, T., Mohr, K., Nicholls, S., Peters-Lidard, C., Posselt, D.J., Skofronick-Jackson, G., 2019. Microphysics in goddard multi-scale modeling systems: a review. In: Randall, D.A., Srinivasan, J., Nanjundiah, R.S., Mukhopadhyay, P. (Eds.), Current Trends in the Representation of Physical Processes in Weather and Climate Models. Springer Atmospheric Sciences. Springer, Singapore, Singapore, pp. 253–316. https://doi.org/10.1007/978-981-13-3396-5_14.

Teixeira, J.C., Carvalho, A.C., Tuccella, P., Curci, G., Rocha, A., 2016. WRF-chem sensitivity to vertical resolution during a saharan dust event. Phys. Chem. Earth, Parts A/B/C 94, 188–195. https://doi.org/10.1016/j.pce.2015.04.002.

Tsarpalis, K., Katsafados, P., Papadopoulos, A., Mihalopoulos, N., 2020. Assessing Desert dust indirect effects on cloud microphysics through a cloud nucleation scheme: a case study over the western mediterranean. Rem. Sens. 12, 3473. https://doi.org/10.3390/rs12213473.

Twomey, S., 1977. The influence of pollution on the shortwave albedo of clouds. J. Atmos. Sci. 34, 1149–1152. https://doi.org/10.1175/1520-0469(1977)034<1149:TIOPOT>2.0.CO;2.

Ukhov, A., Ahmadov, R., Grell, G., Stenchikov, G., 2021. Improving dust simulations in WRF-Chem v4.1.3 coupled with the GOCART aerosol module. Geosci. Model Dev. (GMD) 14, 473–493. https://doi.org/10.5194/gmd-14-473-2021.

Weger, M., Heinold, B., Engler, C., Schumann, U., Seifert, A., Fößig, R., Voigt, C., Baars, H., Blahak, U., Borrmann, S., Hoose, C., Kaufmann, S., Krämer, M., Seifert, P., Senf, F., Schneider, J., Tegen, I., 2018. The impact of mineral dust on cloud formation during the Saharan dust event in April 2014 over Europe. Atmos. Chem. Phys. 18, 17545–17572. https://doi.org/10.5194/acp-18-17545-2018.

Yuan, T., Chen, S., Huang, J., Zhang, X., Luo, Y., Ma, X., Zhang, G., 2019. Sensitivity of simulating a dust storm over Central Asia to different dust schemes using the WRF-Chem model. Atmos. Environ. 207, 16–29. https://doi.org/10.1016/j.atmosenv.2019.03.014.

Zaveri, R.A., Easter, R.C., Fast, J.D., Peters, L.K., 2008. Model for simulating aerosol interactions and chemistry (MOSAIC). J. Geophys. Res. 113, 2007JD008782. https://doi.org/10.1029/2007JD008782.

Zhang, Q., Quan, J., Tie, X., Huang, M., Ma, X., 2011. Impact of aerosol particles on cloud formation: aircraft measurements in China. Atmos. Environ. 45, 665–672. https://doi.org/10.1016/j.atmosenv.2010.10.025.

Zhao, C., Liu, X., Leung, L.R., Johnson, B., McFarlane, S.A., Gustafson, W.I., Fast, J.D., Easter, R., 2010. The spatial distribution of mineral dust and its shortwave radiative forcing over North Africa: modeling sensitivities to dust emissions and aerosol size treatments. Atmos. Chem. Phys. 10, 8821–8838. https://doi.org/10.5194/acp-10-8821-2010.